Materials Letters 253 (2019) 246–249

Contents lists available at ScienceDirect

Materials Letters

journal homepage: www.elsevier.com/locate/mlblue

Sintering of translucent and single-phase nanostructured scandia-stabilized zirconia

Robson L. Grosso [a,b,c,*], Dereck N.F. Muche [b], Taeko Yonamine [d], Eliana N.S. Muccillo [a], Shen J. Dillon [c], Ricardo H.R. Castro [b]

[a] Energy and Nuclear Research Institute, S. Paulo, PO Box 11049, Brazil
[b] Department of Materials Science and Engineering & NEAT ORU, University of California – Davis, CA 95616, USA
[c] Department of Materials Science and Engineering, University of Illinois Urbana-Champaign, Urbana, IL 61801, USA
[d] Institute for Technological Research, S. Paulo 05508-901, Brazil

ARTICLE INFO

Article history:
Received 3 May 2019
Received in revised form 19 June 2019
Accepted 24 June 2019
Available online 24 June 2019

Keywords:
Ceramics
Microstructure
Nanocrystalline materials
Sintering
Phase stabilization

ABSTRACT

Fully-dense and single-phase nanostructured scandia-stabilized zirconia specimens were produced by high-pressure spark plasma sintering technique. Nanocrystalline powders were prepared by the coprecipitation method. Green pellets were sintered at temperatures varying from 700 to 900 °C and pressures from 1.4 to 2 GPa, resulting in dense microstructures with single-phase fluorite-type cubic structure within a wide range of Sc_2O_3 content (6–15 mol%). The average grain size of sintered specimens ranged from 8 to 20 nm. Transmittance spectra confirm translucence in sintered specimens, which is consistent with full density. The results reported here reveal that the polymorphism challenge in the zirconia-scandia system can be successfully suppressed by this consolidation technique, which allows for controlling the grain size of bulk specimens.

1. Introduction

The high versatility and distinct physical-chemical properties of polycrystalline zirconia-based oxides have enabled a wide range of applications, such as refractories, medical prostheses, sensors, and solid electrolytes and electrodes in solid oxide fuel cells (SOFC) [1]. The search for improvements in SOFC devices aiming to decrease operating temperature has motivated investigations on the highest ionic conductivity zirconia-based solid electrolyte, the scandia-stabilized zirconia (ScSZ). ScSZ shows high oxygen ionic conductivity, approximately 2.5× higher than that of yttria-stabilized zirconia (YSZ), very low electronic conductivity in a wide range of oxygen partial pressures, and high chemical stability under oxidizing and reducing atmospheres [1].

Over the last decades, full stabilization of the high ionic conductivity cubic phase at room temperature was accomplished by introducing a second dopant [2–4]. Another approach to stabilize the high symmetry phase at room temperature in powder materials is by decreasing the grain size to the nanoscale [5–7]. A recently proposed phase stability diagram based on thermodynamic considerations, evidenced the feasibility of cubic phase stabilization in the zirconia-scandia system by tuning the grain size [7]. According to this work, 6 mol% Sc_2O_3 is close to the limit of cubic-tetragonal phase stability and rhombohedral phases (β and γ) take place for grain sizes bigger than 25 nm within the range of 10–15 mol%. The size effect on polymorphism was extensively studied in the literature and relates to the role of surface energies on the total energy of the system [8]. It is well established that the presence of a large interface area has also been linked to improvements on physical properties [8–11].

In this work, it is reported for the first time, the preparation of nanostructured bulk specimens of ScSZ (6–15 mol% Sc_2O_3) by high-pressure spark plasma sintering technique using deformable punches, DP-SPS [11]. The consolidated specimens were characterized by optical and microstructural techniques.

2. Experimental

Nanopowders of $(ZrO_2)_{1-x}(Sc_2O_3)_x$ ($6 < x < 15$, represented by *x*ScSZ) were synthesized by coprecipitation. Details on powder preparation and specific parameters may be found elsewhere [7]. Calcined samples were sintered at high pressure using DP-SPS setup [11]. Prior to sintering, powders were degassed at 400 °C overnight. The entire DP-SPS setup was assembled into a glove box under high purity argon atmosphere and inserted in a vacuum

* Corresponding author.
E-mail address: roblopeg@usp.br (R.L. Grosso).

https://doi.org/10.1016/j.matlet.2019.06.076
0167-577X/

chamber of the SPS system (Sumitomo Coal Mining Co., Model 1050). In a typical experiment, the assembly was heat up to 600 °C with 5 min dwell time, using 200 °C.min^{-1} heating rate, followed by a second heating of 50 °C.min^{-1} to the desired temperature. After a specific dwell time, the whole system was naturally cooled down to room temperature. Pressure was applied at 600 °C and increased at constant rate up to the second dwell temperature remaining constant in this last stage. All consolidated specimens were conventional heated at 100 °C below the sintering temperature.

X-ray diffraction (XRD) was used for crystallographic characterization using a Bruker-AXS D8 Advance diffractometer operated with CuKa radiation (λ = 1.5405 Å). Data were acquired from 20° to 80° with 0.03° step size and 5 s.step^{-1} collection time. Phase identification, lattice parameter, and average grain sizes were determined using JADE 6.1 software. Relative sintered density was determined by the immersion method. The theoretical density for each composition was calculated based on lattice parameters. UV–Vis transmittance spectra were recorded using a Thermo Scientific Evolution 220 Spectrometer couple, where blank was recorded previously. The total transmittance was calculated from integrated sphere signal. For transmission electron microscopy (TEM), thin lamellas of sintered specimens were prepared by focused ion beam using Scios 2 Dual-Beam, Thermo Fisher Scientific, with ion source of Ga^+ ions accelerated at 30 kV. TEM images were carried out by using a JEM 2010 LaB_6 (JEOL Ltd.), operating at 200 kV.

3. Results and discussion

Nanopowders of ScSZ were successfully synthesized by coprecipitation method. A total of six compositions within the range of 6–15 mol% Sc_2O_3 was prepared.

Table 1 lists calcination and DP-SPS sintering conditions, crystallite size of calcined powders, and grain size of sintered specimens for each studied composition. The size of the nanoparticles seems to decrease with increasing the Sc_2O_3 content, which can be attributed to the increase of oxygen vacancy concentration, as reported [7,12]. To produce dense specimens with different grain sizes and to verify the influence of the initial particle size on the final grain size, 10.6ScSZ nanopowders were calcined at different temperatures and dwell times, leading to the expected coarsening enhancement for higher temperatures and times as shown in Table 1. After consolidation, all bulk specimens exhibit grain sizes in the nanometer range. The sintering temperature in DP-SPS play a role on the final grain size of ScSZ specimens. This effect is illustrated by the sintering data collected at 800 °C for 4 min at 2 GPa, where the average grain size is around 15 nm independent on the crystallite size or Sc_2O_3 content. No significant influence of the dwell time or pressure (in the studied range) on the grain size was noticeable at a given temperature.

All nanostructured specimens showed relative densities higher than 99%.

Representative photographs of dense ScSZ specimens and optical transmission of selected specimens are shown in Fig. 1. Polished specimens with thicknesses higher than 0.5 mm and diameters close to 3.5 mm exhibit some degree of translucence (Fig. 1a). The room-temperature optical transmission spectra of the fully-dense 10.6ScSZ specimens sintered at 800 °C for 4 min at 1.5 and 2 GPa are depicted in Fig. 1b. Translucency in these specimens can be ascribed to the ultrafine grain size and absence of porosity [9,10], and is, to our knowledge, unprecedented for polycrystalline ScSZ bulk ceramics. Transmission spectra results suggest a significant improvement in translucency when pressure is increased from 1.5 to 2 GPa, which indicates that pressure plays an important role on densification process. As the total forward transmittance accounts in-line and scattered transmitted light as

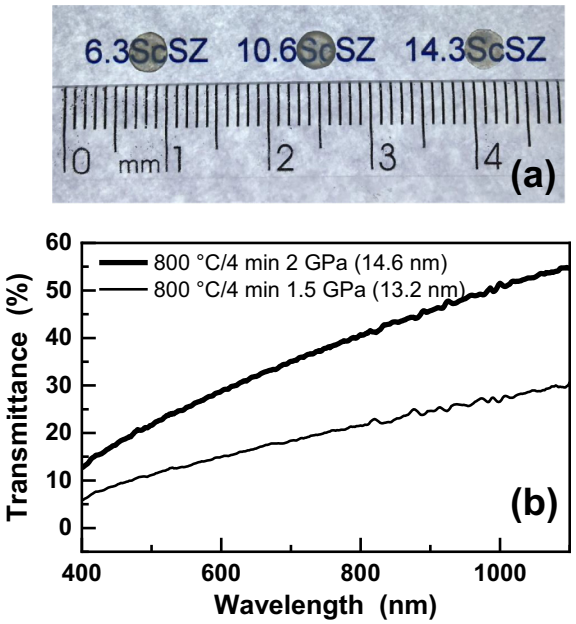

Fig. 1. (a) Photograph of *x*ScSZ (*x* = 6.3, 10.6, and 14.3) specimens consolidated at 800 °C for 4 min at 2 GPa. (b) Optical transmission spectra of 10.6ScSZ specimens.

Table 1
Main characteristics of the powders, DP-SPS conditions, and the average crystallite and grain size (*G*) determined by XRD patterns and TEM images for ScSZ.

Composition	Calcination	Crystallite Size (nm)	Sintering Profile	G_{XRD} (nm)	G_{TEM} (nm)
6.3ScSZ	500 °C/2h	7.9 ± 0.3	800 °C/4 min (2 GPa)	16.1 ± 1.1	15.7 ± 0.6
8.4ScSZ	500 °C/2h	7.7 ± 0.3	700 °C/4 min (1.5 GPa)	8.4 ± 0.6	10.7 ± 0.4
8.4ScSZ	500 °C/2h	7.7 ± 0.3	750 °C/4 min (2 GPa)	11.1 ± 0.7	–
8.4ScSZ	500 °C/2h	7.7 ± 0.3	800 °C/4 min (1.5 GPa)	13.5 ± 0.9	–
8.4ScSZ	500 °C/2h	7.7 ± 0.3	800 °C/4 min (2 GPa)	16.8 ± 1.2	–
8.4ScSZ	500 °C/2h	7.7 ± 0.3	900 °C/4 min (1.5 GPa)	17.0 ± 1.0	–
10.6ScSZ	450 °C/12 h	6.4 ± 0.3	700 °C/16 min (2 GPa)	8.9 ± 0.7	11.3 ± 0.4
10.6ScSZ	450 °C/12 h	6.4 ± 0.3	750 °C/8 min (2 GPa)	12.2 ± 1.7	–
10.6ScSZ	500 °C/2h	7.3 ± 0.3	750 °C/4 min (2 GPa)	10.3 ± 0.6	12.4 ± 0.6
10.6ScSZ	500 °C/2h	7.3 ± 0.3	800 °C/4 min (1.5 GPa)	13.2 ± 0.8	–
10.6ScSZ	700 °C/2h	10.1 ± 0.5	800 °C/4 min (2 GPa)	14.6 ± 1.2	–
10.6ScSZ	700 °C/24 h	12.6 ± 0.3	860 °C/5 min (1.4 GPa)	16.9 ± 1.0	20.6 ± 0.7
11.6ScSZ	500 °C/2h	6.7 ± 0.2	800 °C/4 min (2 GPa)	15.2 ± 0.9	–
12.9ScSZ	500 °C/2h	5.2 ± 0.2	800 °C/4 min (2 GPa)	15.0 ± 0.9	–
14.3ScSZ	500 °C/2h	4.9 ± 0.3	800 °C/4 min (2 GPa)	15.0 ± 1.0	–

well, transparency in some cases might be overestimated. However, although the subtraction of in-line transmittance enables a detailed characterization of optical properties, total transmittance still can be a good tool to provide initial insights on transparency in ceramics [10,13].

Translucence for ScSZ is a positive feature since high density degree is desired for solid electrolyte applications [1]. Considering that polycrystalline ZrO_2-based ceramics are attracting attention as potential optical devices [10,13,14], this characteristic might indicate a new candidate material. However, further studies should be conducted to evaluate ScSZ as an optical device.

An additional factor related to transparency/translucency in ceramics is the crystalline structure and existence of polymorphism. In general, phases with dissimilar refractive indexes will promote light scattering and increased opacity [9,10]. XRD patterns of ScSZ specimens sintered at 800 °C for 4 min at 2 GPa are shown in Fig. 2. For all sintered specimens, only a single-phase fluorite cubic structure was identified in these XRD patterns (Fig. 2a). Fig. 2b shows the angular range between 48 and 53°, usually utilized for identification of the cubic and rhombohedral structures [3–6]. The (2 2 0) diffraction peak is characteristic of the cubic structure.

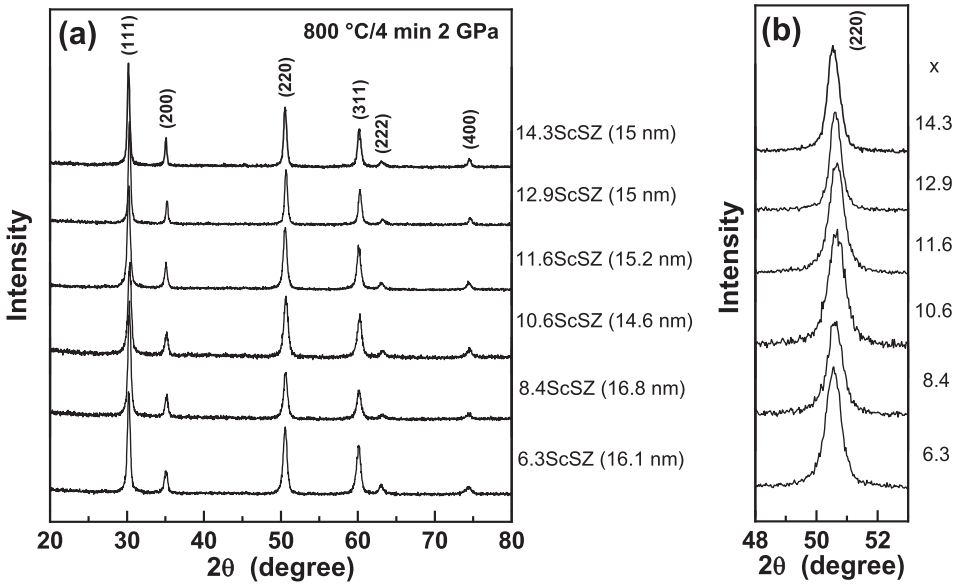

Fig. 2. XRD patterns of the *x*ScSZ specimens sintered by DP-SPS at 800 °C for 4 min at 2 GPa. (a) 20–80° and (b) zooming in the range 48–53°. The average grain size is indicated in the legend.

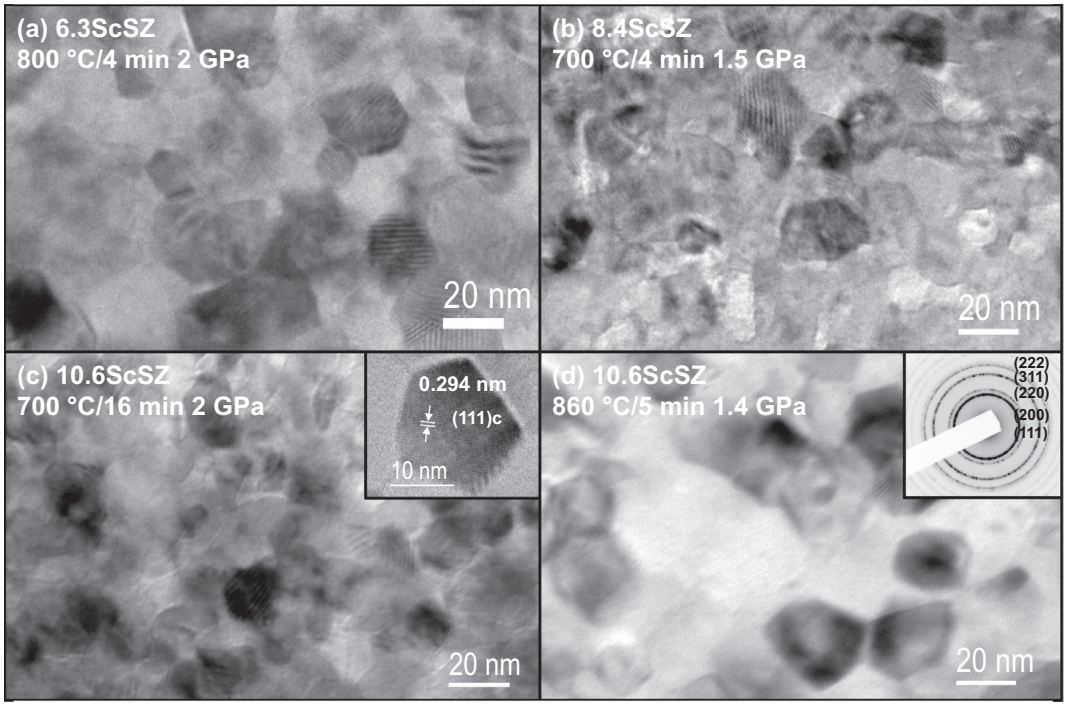

Fig. 3. TEM micrographs of *x*ScSZ specimens sintered by DP-SPS at different conditions: (a) 6.3ScSZ, 800 °C/4 min 2 GPa; (b) 8.4ScSZ, 700 °C/4 min 1.5 GPa; (c) 10.6ScSZ, 700 °C/16 min 2 GPa; (d) 10.6ScSZ, 860 °C/5 min 1.4 GPa.

The determined lattice parameter (5.08 Å) is equal for all investigated compositions, corroborating the effect of grain size on phase stabilization of ScSZ.

TEM micrographs of ScSZ sintered specimens are depicted in Fig. 3. The images evidence the nanocrystalline grain size, full density, and high degree of microstructural homogeneity within a wide range of Sc_2O_3 content. The average grain size determined from TEM images are similar to those calculated from XRD patterns (Table 1). The observed differences may be attributed to the difficulty in measuring smaller grain sizes by TEM images due to grain superposition in two-dimensional images. No cation segregation was detected, as evidenced by high-resolution image (inset Fig. 3c). Interplanar distance of 0.294 nm, which corresponds to (1 1 1) plane of the cubic fluorite phase was measured. The electron diffraction pattern ensures cubic phase stabilization after sintering (inset Fig. 3d). Grain sizes are below 20 nm for all specimens promoting stabilization of the cubic phase. These results agree with the recently reported phase diagram of ScSZ nanoparticles [7].

Overall, the results suggest that DP-SPS shall be considered an alternative to the current state-of-the-art graphite SPS setup since full density can be achieved in nanograin sized ceramics. However, a setup should be designed to produce larger pieces.

4. Conclusion

Fully-dense translucent nanostructured ScSZ specimens within a wide range of Sc_2O_3 content (6–15 mol%) with grain size as small as 8 nm were successfully produced by DP-SPS. Fluorite-cubic phase stabilization at room temperature was confirmed by X-ray diffraction and electron diffraction pattern. The results confirmed the grain-size dependent phase stability in zirconia-scandia system also in the sintered dense form.

Declaration of Competing Interest

The authors declare no conflict of interest.

Acknowledgements

The authors gratefully acknowledge FAPESP (2016/06205-1 and 2017/25501-3), CAPES (Finance code 001) and CNPq (305889/2018-4 and 236631/2012-8). RC acknowledges Army Research Office Grant W911NF-17-1-0026 for the financial support. TEM analysis were carried out in the Frederick Seitz Materials Research Laboratory Central Research Facilities, University of Illinois.

References

[1] S.P.S. Badwal, F.T. Ciacchi, Oxygen-ion conducting electrolyte materials for solid oxide fuel cells, Ionics 6 (2000) 1–21, https://doi.org/10.1007/BF02375543.
[2] S. Omar, W.B. Najib, W. Chen, N. Bonanos, Electrical conductivity of 10 mol% Sc_2O_3-1 mol% M_2O_3-ZrO_2 ceramics, J. Am. Ceram. Soc. 95 (2012) 1965–1972, https://doi.org/10.1111/j.1551-2916.2012.05126.x.
[3] R.L. Grosso, R. Muccillo, E.N.S. Muccillo, Stabilization of the cubic phase in zirconia-scandia by niobium oxide addition, Mater. Lett. 134 (2014) 27–29, https://doi.org/10.1016/j.matlet.2014.07.039.
[4] J.P. Souza, R.L. Grosso, R. Muccillo, E.N.S. Muccillo, Phase composition and ionic conductivity of zirconia stabilized with scandia and europia, Mater. Lett. 229 (2018) 53–56, https://doi.org/10.1016/j.matlet.2018.06.091.
[5] G. Xu, Y.W. Zhang, C.S. Liao, C.H. Yan, Doping and grain size effects in nanocrystalline ZrO_2-Sc_2O_3 system with complex phase transitions: XRD and Raman studies, Phys. Chem. Chem. Phys. 6 (2004) 5410–5418, https://doi.org/10.1039/b413701a.
[6] M. Okamoto, Y. Akimune, K. Furuya, M. Hatano, M. Yamanaka, M. Uchiyama, Phase transition and electrical conductivity of scandia-stabilized zirconia prepared by spark plasma sintering process, Solid State Ionics 176 (2005) 675–680, https://doi.org/10.1016/j.ssi.2004.10.022.
[7] R.L. Grosso, E.N.S. Muccillo, R.H.R. Castro, Phase stability in scandia-zirconia nanocrystals, J. Am. Ceram. Soc. 100 (2017) 2199–2208, https://doi.org/10.1111/jace.14710.
[8] R.H.R. Castro, On the thermodynamic stability of nanocrystalline ceramics, Mater. Lett. 96 (2013) 45–56, https://doi.org/10.1016/j.matlet.2013.01.007.
[9] G.L. Messing, A.J. Stevenson, Toward pore-free ceramics, Science 322 (2008) 383–384, https://doi.org/10.1126/science.1160903.
[10] L.B. Kong, Y.Z. Huang, W.X. Que, T.S. Zhang, S. Li, J. Zhang, Z.L. Dong, D.Y. Tang, in: Transparent Ceramics, Springer International Publishing, Switzerland, 2015, https://doi.org/10.1007/978-3-319-18956-7.
[11] D.N.F. Muche, J.W. Drazin, J. Mardinly, S. Dey, R.H.R. Castro, Colossal grain boundary strengthening in ultrafine nanocrystalline oxides, Mater. Lett. 186 (2017) 298–300, https://doi.org/10.1016/j.matlet.2016.10.035.
[12] R.L. Grosso, E.N.S. Muccillo, R.H.R. Castro, Enthalpies of formation in the scandia-zirconia system, J. Am. Ceram. Soc. 100 (2017) 4270–4275, https://doi.org/10.1111/jace.14945.
[13] J. Klimke, M. Trunec, A. Krell, Transparent tetragonal yttria-stabilized zirconia ceramics: influence of scattering caused by birefringence, J. Am. Ceram. Soc. 94 (2011) 1850–1858, https://doi.org/10.1111/j.1551-2916.2010.04322.x.
[14] U. Anselmi-Tamburini, J.N. Woolman, Z.A. Munir, Transparent nanometric cubic and tetragonal zirconia obtained by high-pressure pulsed electric current sintering, Adv. Funct. Mater. 17 (2007) 3267–3273, https://doi.org/10.1002/adfm.200600959.